Solution Structure of the Aminoacyl-Capped Oligodeoxyribonucleotide Duplex (W-TGCGCAC)$_2$[†]

William C. Ho, Christoph Steinbeck,[‡] and Clemens Richert*

Department of Chemistry, Tufts University, 62 Talbot Avenue, Medford, Massachusetts 02155

Received May 20, 1999; Revised Manuscript Received July 30, 1999

ABSTRACT: Reported here is the solution structure of the aminoacyl-DNA duplex (W-TGCGCAC)$_2$. This duplex forms a continuously π-stacked helix consisting of both nucleobases and amino acid side chains. According to NMR and UV analyses, the duplex melts in a cooperative transition and with 1.3−1.8% greater hyperchromicity than the control duplex (TGCGCAC)$_2$. A van't Hoff analysis of UV melting points at different concentrations shows that the two tryptophan residues contribute 4.8 kcal/mol to the $\Delta H°$ of complex formation at 10 mM salt concentration and less than 1 kcal/mol at 150 mM salt. The entropic cost for duplex association in the presence of the amino acid residues is 13 cal/molK greater than that for the control at 10 mM salt concentration, and 3 cal/molK lower than that of the control at 0.15 ionic strength. The conformation of W-TGCGCAC in duplex form, determined via restrained torsion angle molecular dynamics, shows an undisturbed B-form DNA duplex with dangling 3′-termini. The tryptophanyl residue at the 5′-terminus packs tightly against T2 and the proximal part of adenine, without engaging in hydrogen bonding. While not providing strong enthalpic net stabilization of the duplex, the tryptophan "cap" on the duplex does seem to reduce the fraying at the termini, indicating a subtle balance of entropic and enthalpic factors contributing to the molecular dynamics. The structure also shows that, at least in the present sequence context, stacking on the terminal base pair is more favorable than intercalation, probably because the enthalpic cost associated with breaking up the stacking between DNA base pairs cannot be paid for by favorable π-stacking interactions with the indole ring of tryptophan. These results are of importance for understanding stacking interactions in protein−DNA complexes, particularly those in enzyme−substrate complexes involving exposed nucleobases.

Noncovalent interactions between amino acid residues and nucleic acids form the basis of protein−DNA interactions and are thus central to the expression, replication, and repair of genetic information. Two classes of amino acid residues are frequently found on the contact surfaces of protein−DNA complexes: cationic and aromatic residues. For cationic residues, whose interactions with DNA are dominated by ion pair formation and hydrogen bonding, model peptides with measurable affinity for double-stranded DNA are available (*1*). For aromatic amino acid residues, such as tryptophan, the design of such model peptides is more difficult. Their possible interactions with DNA are more complex and usually require the context of a folded structure, due to their hydrophobicity. On the basis of high-resolution structures of DNA−protein complexes, it appears that nature does not favor complete intercalation of tryptophan into double-stranded DNA (*2*−*6*). For partial intercalation, wedges built from combinations of aromatic and nonaromatic amino acids (*7*, *8*) or nonaromatic amino acids alone (*9*) are more typical. Examples for interactions of tryptophan side chains with DNA also include stacking on exposed nucleobases and hydrogen bonding with nucleobases or phosphodiesters (*10*−*14*), making it difficult to predict the DNA interactions of a tryptophan residue unconstrained by a given protein fold. For other indole derivatives, such as diaminidino-2-phenylindole (DAPI) (*15*), the situation is similarly complex, since both intercalation and minor groove binding have been reported (*16*, *17*).

For short model peptides containing cationic and aromatic amino acids, it has been proposed that side chains of aromatic amino acids do intercalate or partially intercalate into dsDNA[1] (*18*−*27*), and evidence for intercalation has been presented for a tryptophan derivative bound to a short DNA duplex (*28*). Further, extensive spectroscopic studies have relied on fluorescence quenching observed when tryptophan-containing peptides interact with DNA (*29*−*32*).

We have studied the effect of aminoacylation of oligodeoxyribonucleotides on their binding to RNA targets (*33*). In this context, we measured a change in target affinity resulting from 5′-tryptophanyl-residues. Since the affinity of Trp alone for DNA is low (*34*), we reasoned that the more subtle hydrophobic and π-stacking interactions between tryptophan and nucleobases could be studied in complexes of tryptophan-bearing DNA, where the peptide linkage entropically favors and thus facilitates interactions between the aromatic

[†] Supported by the NIH, National Institutes of General Medical Sciences, Grant GM54783 to C.R. The Center for Magnetic Resonance at the Francis Bitter Magnet Laboratory, MIT, is supported by Grant RR00995 from the National Center for Research Resources at the NIH. The upgrade of an NMR spectrometer at Chemistry Department at Tufts University is supported by NSF Grant CHE-9723772 (to C.R. and M. d'Alarcao).

* To whom correspondence should be addressed.

[‡] Current address: Max-Planck-Institute for Chemical Ecology, D-07745 Jena, Germany.

[1] Abbreviations: dsDNA, double-stranded DNA; T_m, melting point.

10.1021/bi991169w CCC: $18.00 © 1999 American Chemical Society
Published on Web 09/09/1999

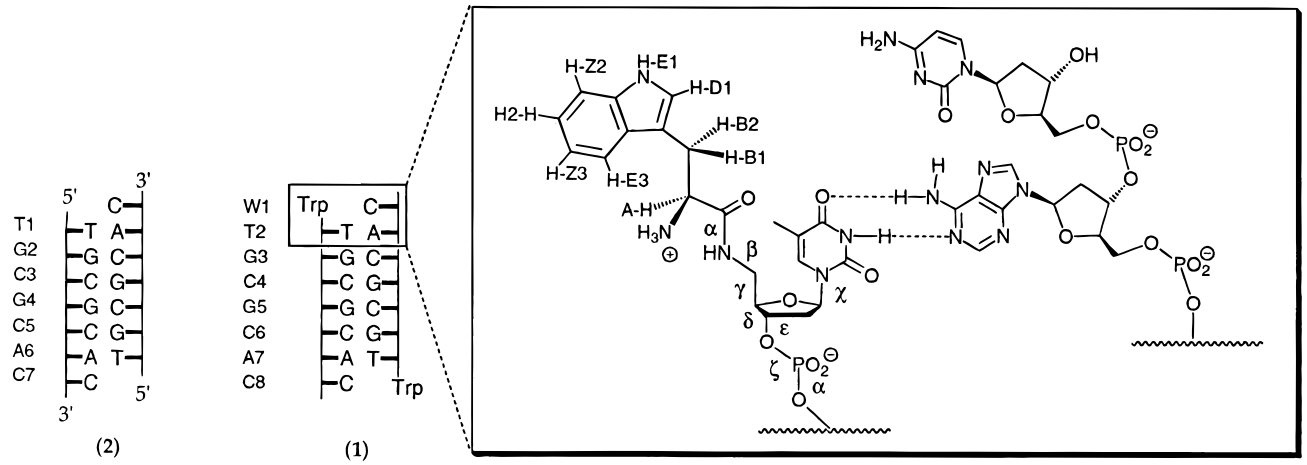

FIGURE 1: Schematic drawing of the compounds employed in this work. The highlighted box shows the site of aminoacylation with the naming scheme and angle nomenclature used.

rings of the amino acid side chain and the nucleobases, but does not restrict it in a tight fold. Here we report the solution structure of the duplex of the self-complementary 5′-tryptophanyl oligonucleotide W-TGCGCAC, together with the thermodynamic parameters derived from UV melting studies on this duplex (**1**) and its control DNA duplex (**2**) (Figure 1).

The self-complementary hexamer in **1** bears two terminal residues: the tryptophanyl residue appended to the 5′-end via a peptide bond and a cytidine residue at the 3′-terminus. For these, a number of different interaction modes, such as intercalation, hemi-intercalation, displacement intercalation, or edge-on- or face-on-stacking on the terminal base pair, were considered. Molecular dynamics showed that at least three of the principal forms of interaction were conformationally accessible for W1 (Figure 2). The structure solved via restrained molecular dynamics shows the tryptophan (but not the cytidine residue) stacked on the terminal base pair. The well-defined stacking array does not involve any hydrogen bonds to the tryptophan residue.

MATERIALS AND METHODS

Synthesis of W-TGCGCAC and Control Heptamer TGCGCAC. Oligonucleotides were synthesized on 10 μmol scale (W-TGCGCAC, **1**) or 3 μmol scale (TGCGCAC, **2**) on an ABI 381A DNA synthesizer. Phosphoramidites for the naturally occurring nucleotides dA^{Bz}, dC^{Bz}, and dT (ABI/Perkin-Elmer), dG^{DMF} (Glen Research), and Fmoc-Trp-OH (Advanced ChemTech) were used as received. The tryptophan-bearing oligonucleotide **1** was produced by coupling Fmoc-Trp-OH to protected, 5′-amino-terminal DNA on controlled pore glass with HBTU/HOBT/DIEA activation in DMF, followed by basic deprotection with ammonium hydroxide, according to a procedure previously described (*35*). Oligonucleotides were purified by RP-HPLC on either C-18 or C-4 phases with 0.1 M triethylammonium acetate solution, pH 7.0, and a gradient of CH_3CN. On a C-18 phase, aminoacylated oligonucleotide W-TGCGCAC (**1**) eluted after 30.5 min with a gradient of 0% CH_3CN for 5 min and 0 to 20% CH_3CN in 30 min. On a C-4 phase with a gradient of 0% CH_3CN for 5 min and 0% to 22% CH_3CN in 20 min, **1** eluted after 25 min. Control compound **2** eluted after 22.6 min, when chromatographed on a C-18 phase with 0% CH_3CN for 3 min and a gradient from 0 to 18% CH_3CN in 27 min. MALDI-TOF MS, negative mode, external calibration; W-TGCGCAC (**1**) calcd for $C_{78}H_{97}N_{29}O_{40}P_6$, 2266.6 (average mass); found, 2266 ± 2 ($[M - H]^-$); (**2**) TGCGCAC calcd

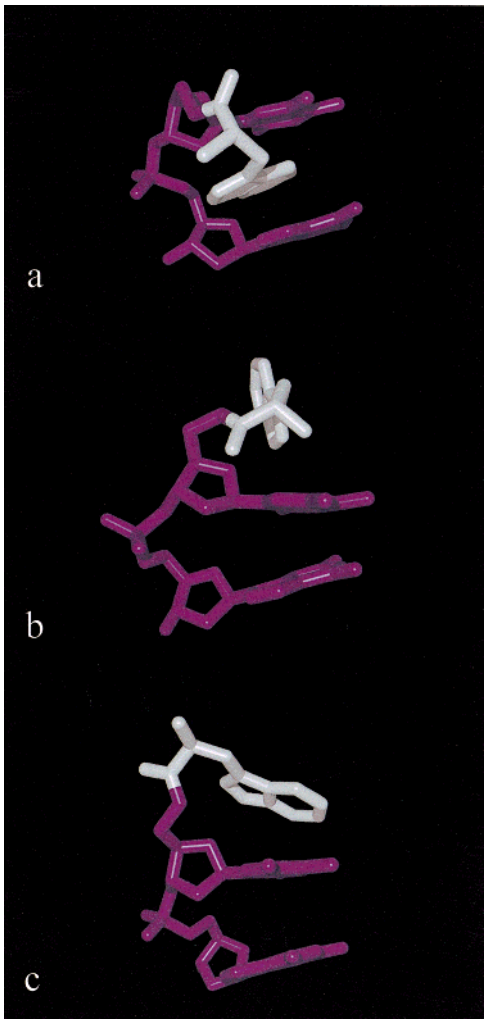

FIGURE 2: Comparison of three selected conformationally accessible interaction modes of W1 with the 5′-terminal DNA portion of $(W\text{-}TGCGCAC)_2$. Force field minimized conformations obtained with nonexperimental constraints. (a) Partial intercalation of the indole ring, (b) stacking of the linker with solvent-exposed indole ring, (c) stacking of the indole ring on the terminal base pair. Residue W1 is white, residues T2 and C3 are purple.

Table 1: UV-Melting Points and Hyperchromicities

duplex	salt concentration (mM)	T_m (°C)[a]	hyperchromicity (%)
1	10	23.0 ± 0.6	8.6
2	10	18.5 ± 0.3	7.3
1	150	36.3 ± 0.6	9.8
2	150	34.2 ± 0.9	8.0

[a] Average of four melting points at 12 μM strand concentration ± 1 SD.

for $C_{67}H_{86}N_{26}O_{40}P_6$, 2081.4; found, 2081 ± 2 ([M − H]$^-$).

UV Melting Curves and Thermodynamic Data. Melting and cooling curves were measured at 260 nm in 1 or 0.2 cm optical path-length cuvettes on a Perkin-Elmer Lambda 10 spectrophotometer equipped with a C6+ Peltier-thermostated programmable autolinear transport multicell holder driven by a PTP-6 temperature controller, and a temperature sensor in cuvette 1. Oligonucleotide solutions in DEPC-treated water (Ambion), ranging from 1.3 to 90 μM in strand concentration, containing 0.1 mM EDTA and the desired concentration of ammonium acetate salt (Ambion) were used. Melting curves were acquired at heating or cooling rates of 1 °C/min between 5 and 65 °C. Background absorbance changes were determined from the concurrent acquisition of a control sample containing buffer alone. Melting points were determined with UV TempLab 1.2. Curves were smoothed with a 95 point moving average and melting points taken as the extrema of the 91 point first derivative. At least three melting points were measured at every oligonucleotide concentration, and the average was used for van't Hoff plots. The standard deviation for the melting points was between 0.3 and 1.8 °C (Table 1 gives representative data at 12 μM strand concentration). Thermodynamic parameters were determined from ln c_t versus $1/T_m$ plots (see Supporting Information) using $1/T_m = (R/\Delta H°)\ln c_t + \Delta S°/\Delta H°$, where T_m is the melting point, c_t is the total strand concentration, and R is the molar gas constant (8.3145 J mol^{-1} K^{-1}) (*36*).

Sample Preparation for NMR Spectroscopy. HPLC-purified and lyophilized W-TGCGCAC was taken up in 5% ammonium hydroxide and relyophilized five times to remove residual triethylamine. Samples were prepared by dissolving the residue either in 99.999% D_2O or in H_2O/D_2O (9:1) containing 150 mM NaCl and 10 mM phosphate buffer (KH_2PO_4/K_2HPO_4) at pH 7.0 (uncorrected for deuterium effect). Residual heavy metal contaminations were precipitated by treatment with H_2S and centrifugation. Sample volumes of 250 ± 10 μL in microtubes (Shigemi Co., Tokyo, Japan) were used for NMR spectroscopy. Changes between D_2O and H_2O were brought about by evaporation and redissolving in the solvent of choice. The final concentration of the oligonucleotides in the NMR solution was 4 mM.

NMR Spectroscopy. NMR spectra were recorded on Bruker AM 300 and AVANCE 300 spectrometers (1D experiments at different temperatures and exploratory NOESY experiments), Bruker AMX 500 and DPX 600 spectrometers, and 500 and 750 MHz spectrometers custom designed at the Francis Bitter Magnet Laboratory, Massachusetts Institute of Technology, Cambridge, MA. Experiments in D_2O were performed with suppression of the residual solvent peak by presaturation for 1.5 s during the recycle delay. Experiments in H_2O/D_2O used presaturation (1.3 s, AMX 500) or a WATERGATE gradient pulse sequence (*37*) (custom-built spectrometers). A series of NOESY (*38*) spectra at 40, 80, 160, 320, and 500 ms mixing time was acquired with WATERGATE water suppression at 10 °C and 10 000 Hz sweep width, as well as a TOCSY (*39*) (80 ms spin lock time), and DQF-COSY (*40*) spectra at 5800 Hz spectral width at the same temperature, together with a NOESY spectrum with presaturation at 300 ms mixing time, 20 °C and 9090 Hz sweep width. Spectra in D_2O (NOESY at 320 ms mixing time, DQF-COSY, and TOCSY at 120 ms spin lock time) were acquired at 10 °C with 6000 Hz spectral width. Spectra were collected with 4096 data points in t_2, 256, or 512 increments in t_1, and 24, 32, or 64 scans/increment. Recycle delays were 2 s. Chemical shifts were calibrated to TPS at 0.0 ppm.

Generation of Restraints for Molecular Dynamics. Spectra were processed using GIFA (*41*). Two-dimensional spectra were zero-filled to 2048 data points in t_1, followed by first-point correction and apodization with Gaussian line broadening and exponential line narrowing. Peak assignment started from the methyl group of T2, whose TOCSY cross-peak to H6 of T2 produced the starting point for sequential assignment of H1′/H6/8 resonances in the NOESY spectra, as described in the Results (vide infra). Coupling constants for H-1′ protons (H1′−H2′ and H1′−H2″) were read from a one-dimensional spectrum at 300 MHz and were checked with those derived from DQF-COSY cross-peaks (*42*) for the partially overlapping resonances of A7 and C8.

For generating distance constraints, NOESY cross-peaks were integrated using the Gaussian line-shape approximation. All line fits of integrals were visually controlled for accuracy. The intensity of partly overlapping peaks was estimated by visual inspection. Build-up curves were generated for 12 representative cross-peaks from NOESY spectra acquired at mixing times of 40, 80, 160, 320, and 500 ms in H_2O/D_2O at 10 °C. A monotonic rise in cross-peak intensity was observed up to 320 ms mixing time for all but the exchangeable protons and cross-peaks between geminal coupling partners. The latter were not used for restrained molecular dynamics, as the relative position of these protons is already well-defined by the force field. Constraints for cross-peak to H1′, H2′, H2″, and most resonances of W1 were read from the 320 ms NOESY spectrum from the H_2O/D_2O solution. Calibration of distance constraints via the two-spin approximation was initially based on H5/H6 cross-peaks of cytidine residues (2.45 Å). After it was established that a B-type duplex was present [based on the correlation of 21 representative relative cross-peak intensities with those predicted for B-form DNA (*43*), the coupling constants found for the H1′ resonances, and the cross-peak intensity of the H1′ to H6/8 cross-peaks] the calibration relationship was refined by a least-squares fit to the average of H2′-C to H8-G and H1′-C to H6/8-C/G cross-peak intensities at their ideal B-DNA distances. Cross-peaks from the terminal base pairs were not used for this refining of the calibration. Distances read from the calibration function were treated with error bars of ±0.4 Å for $r_{ij} < 3.5$ Å and ±0.5 Å for $r_{ij} > 3.5$ Å. Cross-peaks whose overlap with neighboring peaks required estimation were provided with error bars of ±1.0 Å, without allowing distances below van der Waals contact. Constraints involving HE1 of W1 were treated the same as nonexchangeable protons, and those involving the amide proton of the peptide linkage were treated with errors of ±1.0 Å.

Table 2: Thermodynamic Parameters for Duplex Dissociation of $(W\text{-}TGCGCAC)_2$ and Control Duplex $(TGCGCAC)_2$, as Derived from van't Hoff Analysis of ln c_t versus $1/T_m$ Plots

duplex	salt concn	$\Delta H°$ (kcal/mol)	$\Delta S°$ (cal/molK)	$\Delta G°$ (kcal/mol)
$(TGCGCAC)_2$	10	38.6	110	5.8
	150	42.8	116	8.1
$(W\text{-}TGCGCAC)_2$	10	43.4	123	6.6
	150	42.0	113	8.3

Distance constraints for H3′ and H5′/5″ protons, as well as those for HA of W1 could not be obtained in the H_2O/D_2O spectra due to signal loss caused by the WATERGATE water suppression. These were obtained from NOESY spectra in D_2O and otherwise identical solvent conditions as those for water spectra, using calibration functions obtained in an analogous fashion. Additional cross-peaks for HH2 and HZ3 were also obtained from the D_2O spectra and were assigned to one of the two after refined structures were obtained in an iterative process guided by structure quality. Table 4 gives an overview over the constraint data used.

Structure Generation. Calculations leading to the final set of low-energy structures were performed with CNS, version 0.4, courtesy of Drs. Brünger and Grosse-Kunstleve, Yale University. Details of the computational approach are given in Table 5. Diasterotopic protons that could not be stereoselectively assigned, as well as the methyl group at position 5 of thymine, were treated with the geometric center pseudoatom approach, which results in a greater tolerance of distance constraints derived from NOESY cross-peaks. One cross-peak to the methyl group of T2 did not agree with any of the otherwise constraint-violation free structures and was excluded from the calculations. Initial structures were calculated with NOE-based constraints and hydrogen-bonding constraints for the core duplex only. While the correct fold of the duplex was produced under these conditions, the rmsd of coordinates was unsatisfactory. After a B-type conformation of the DNA duplex had been established (vide supra), backbone dihedral angles of DNA residues 2−7 were constrained using the parameters from X-PLOR and CNS. This led to better defined structures and improved agreement between the back-calculated and experimental NOESY spectrum. Back-calculations were performed with the rigid body two-spin approximation tool of X-PLOR and spectra were generated with GIFA. The agreement between theoretical and experimental spectra improved further when base pair planarity constraints with a low-energy penalty (10 kcal/mol) were introduced. Statistics on the 10 lowest energy structures obtained from the restrained molecular dynamics are given in Table 6.

RESULTS

Synthesis and UV-Melting Experiments. The synthesis and purification of $(W\text{-}TGCGCAC)_2$ were performed using previously published methodology (*35*) and proceeded uneventfully. UV-melting points were obtained for both **1** and **2** at all concentration points between 1.3 and 90 μM strand concentration and at both 10 and 150 mM salt, with the exception of the low salt melting point of **2** at 1.3 μM total strand concentration. Representative melting points and curves are shown in Table 1 and Figure 3, and ln c_t versus $1/T_m$ plots with all data points are shown in the Supporting Information. The values obtained for **2** are close to those predicted using nearest neighbor data for the core duplex 5′-TGCGCA-3′ (33.9 °C at 1 M NaCl and 5 μM total strand concentration) (*44*). At low salt, aminoacylated **1** shows a melting point 4.5 °C higher than that of **2**. At 150 mM salt, this increase in melting point is reduced to 2.1 °C, i.e., +1.1 °C/aminoacylation. The latter value is identical to the +1.1 °C measured in a nonself-complementary DNA octamer binding to an RNA undecamer (*33*). The melting points of **1** were high enough for NMR analysis of the complex at or below room temperature, but low enough to allay concerns (*45*) over extrapolation of thermodynamic parameters obtained at close to boiling point to equilibria at room temperature.

Table 3: Chemical Shifts (ppm) of Aromatic Protons in **1** and Control Compounds

proton[a]	H-Trp-OH[b]	**1** at 10 °C[c]	**1** at 90 °C[c]	**2** at 10 °C[c]
W1				
H−D1	7.26	6.91	7.19	
H−E3	7.67	7.10	7.54	
H−Z2	7.48	6.88	7.42	
H−H2	7.14	6.61	7.06	
H−Z3	7.23	6.61	7.15	
T2				
H-6		7.19	7.14	7.45
G3				
H-8		8.04	7.89	8.09
C4				
H-5		5.44	5.86	5.46
H-6		7.43	7.64	7.42
G5				
H-8		7.89	7.68	7.95
C6				
H-5		5.34	5.85	5.49
H-6		7.07	7.59	7.35
A7				
H-2		7.84	8.14	7.84
H-8		8.22	8.32	8.25
C8				
H-5		5.94	5.95	5.85
H-6		7.80	7.79	7.72

[a] Residue numbering is that of **1**. [b] L-Tryptophan in D_2O. [c] In D_2O, 150 mM NaCl and 10 mM phosphate buffer.

Table 4: Constraints Used for Calculating the Three-Dimensional Structure of **1**

NOE restraints[a]	
total	74
interresidue	35
intraresidue	39
interresidue for W1	9
intraresidue for W1	9
dihedral angle restraints	53
hydrogen bond restraints	8
base pair planarity restraints	6

[a] Due to the symmetrical nature of the duplex, all constraints except base pair planarity constraints were applied to both strands individually, so that the number of actual constraints is twice that given.

The influence of the tryptophan appendage on the thermodynamics of the UV transition were used to obtain quantitative data on the strength of the interactions between the aminoacyl appendage and the DNA. van't Hoff analysis of $1/T_m$ versus ln c_t plots gave a $\Delta\Delta H$ of +4.8 kcal/mol for the tryptophan-bearing duplex at low salt and a $\Delta\Delta H$ of −0.8 kcal/mol at 150 mM salt (Table 2). Since the standard deviation of the individual melting points was on average ±0.8 °C and the plots gave r^2 factors of between 0.985 and 0.998, we estimate that the latter $\Delta\Delta H$ value is close to the experimental error. Entropically, involving the tryptophan

Table 5: Parameters of the Molecular Dynamics Calculations Employed for Determining the Three-Dimensional Structure of **1**

	high-temperature torsion-angle molecular dynamics	slow-cooling torsion-angle molecular dynamics	slow-cooling Cartesian molecular dynamics	40 000 steps conjugate gradient minimization
temp (K)	20 000	20 000 to 0	1000 to 0	
time step (ps)	0.15	0.015	0.003	
Δt (ps)	60	15	6	
w_{NOE}	150	150	150	50
$w_{dihedral}$	5	5	100	300
w_{vdw}	1.0	0.1 to 1.0	1.0	1.0

Table 6: Quality Data on the Ten Lowest Energy Structures of **1** Obtained from Torsion Angle Molecular Dynamics

restraint violation	
NOE violations	0 (>0.5 Å)
dihedral angle violations	0 (>12 °)
H-bond violations	0
deviation from ideal geometry	
bond distances	0 (>0.05 Å)
bond angles	0 (> 5 °)
refinement statistics for 10 final lowest energy structures	
rmsd from average[a]	0.68 Å
pairwise rmsd of coordinates[a]	1.2 Å
pairwise rmsd angles[a]	0.69 Å
pairwise rmsd of bond lengths[a]	0.004 Å
energy	-126 ± 2 kcal/mol

[a] The disordered residue C8 is part of the structures analyzed.

residue in complex formation costs a $\Delta\Delta S$ of 13 cal/mol K at low salt, according to the van't Hoff data, and has a negligible effect (−3 cal/mol K) at the higher salt concentration.

The UV hyperchromicity accompanying duplex dissociation is only 7.3% for heptamer **2** at 10 mM salt concentration (Figure 3 and Table 1), a value well below the 20−35% typically obtained for polymeric DNA. This is most probably due to extensive breathing of the termini and thus incomplete base stacking in the short duplex. Compared to **2**, aminoacylated **1** shows a 1.18-fold increased hyperchromicity. This effect is also observed at 150 mM salt (1.23-fold higher hyperchromicity for **1** than **2**), where the shielding of the phosphodiester anions by counterions reduces charge−charge repulsion and facilitates a tight packing of the strands. Even though the increases in hyperchromicity are small, they are outside the experimental error and demonstrate an effect of the tryptophanyl cap on the stacking in the duplex.

Resonance Assignments and One-Dimensional NMR Data. In a B-form DNA helix, the H8 and H6 protons of the nucleobases give NOESY cross-peaks to both the H1′ of their own nucleotide and the H-1′ of their 5′-neighboring nucleotide (*46*−*48*). This sequential connectivity was found for nucleotides T2−A7 of **1** in phosphate-buffered saline at 10 °C (Figure 4b). The resonances of H2 and H8 of A7, both of which give cross-peaks to H1′ of A7, could be unambiguously assigned by exchanging the H8 proton for a deuterium through heating a D_2O solution to the boiling point for 1 h (*49*). The cross-peak from H8-A7 to H1′-C8 was difficult to find because of an overlap between H1′-A7 and H1′-C8. Deletion analysis of the H6/H5 spin systems of cytidines in the DQF-COSY was therefore used to identify the aromatic protons of C8. With the exception of H5′/5″ of C4, all nonexchangeable protons of the ribose spin systems and of the tryptophan residue were then assigned based on DQF-COSY and NOESY cross-peaks as detailed in the Materials and Methods. Chemical shifts for HH2 and HZ3 of W1 and H2′/2″ of G5 were found to be identical. Imino resonances of G3 and G5, amino resonances of C4 and C6, and the HE1 resonance of W1 were picked in NOESY spectra acquired in H_2O/D_2O (9:1). The amino and imino resonances were connected to resonances of nonexchangeable protons via NOESY cross-peaks of H42 to H5 of cytidines and HE1-W1 and NH5′-T2 to HD1-W1 and H5′/H5″-T2, respectively. An assignment table is given in the Supporting Information.

All H1′ resonances, except those of A7 and C8, were discernible as triplets or doublets of doublets at 300 MHz and room temperature, with coupling constants between 5.5 and 8.9 Hz. The H1′ to H2′ and H2″ coupling constants of A7 and C8 were derived from DQF-COSY cross-peaks. The coupling constants indicated that all ribose rings were in 2′-endo conformation, as expected for a B-form duplex (*50*). Further confirmation for an undisturbed B-form DNA duplex came from the DQF-COSY cross-peak pattern between H2′/2″ and H3′ of all nucleosides.

Compared to unconjugated tryptophan, all protons of W1 show significantly shifted resonances (Table 3). For HA, the shift is toward lower field, as expected for the conversion from a free carboxylate to the amide-bound form. For all other protons, resonances shift to higher field, as expected for close proximity to nucleobases with magnetic anisotropy effect. The high-field shift is more pronounced for hydrogens at the six-membered ring (between 0.53 and 0.62 ppm) than for HD1 of the pyrrole ring unit (0.35 ppm).

A detailed chemical shift analysis was performed for all aromatic protons after acquiring spectra of control duplex **2** at 10 °C, whose resonances were assigned analogously to those of **1**, and of aminoacylated duplex **1** at 90 °C, where a random-coil conformation can be assumed. The one-dimensional spectra are shown in the Supporting Information. For W1, the chemical shifts at 90 °C are very similar to those of free L-tryptophan ($\Delta\delta \leq 0.13$ ppm), confirming that the upfield shifts in the duplex form of **1** are the result of stacking interactions. For T2, an upfield shift of 0.26 ppm is observed for H6 compared to **2** at 10 °C, indicating the effect of an additional aromatic ring current, most probably that of W1. For A7, shifts for H2 and H8 are similar to those in **2**. For H8 of G3, there is little chemical shift difference between duplex forms of **1** and **2**, but for C6, an upfield shift of 0.15 and 0.28 ppm, respectively, is observed for H5 and H6 (−0.28 ppm) upon aminoacylation. Further, a greater shift difference between duplex and single-stranded form is seen for C6 than for C4 (+0.51 ppm for H5 and +0.52 ppm for H6 versus 0.42 and 0.21 ppm of the same resonances in C4), indicating the influence of an additional aromatic ring. The protons of the internal base pair, C4 and G5, are very similar for **1** and **2** in duplex form (≤0.07 ppm), pointing to an unperturbed interior of the duplex.

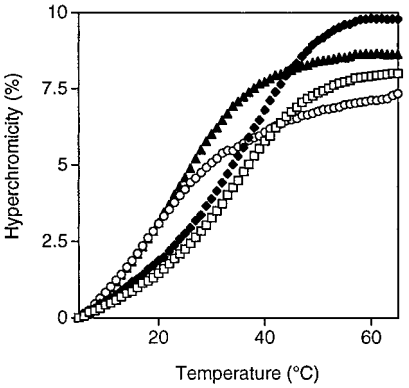

FIGURE 3: UV melting profiles (260 nm) of $(TGCGCAC)_2$ (**2**) at 10 mM (○), and 150 mM salt (□), together with those of W-TGCGCAC (**1**) at 10 mM (▲), and 150 mM salt (◆).

For C8, there is virtually no difference between the chemical shifts of the aromatic protons in **1** at 10 and 90 °C ($\Delta\delta$ 0.01 ppm), indicating that the nucleobase does not stack on an aromatic moiety at 10 °C. This is also apparent from the narrower line widths of H5 and H6 of C8 at 10 °C, compared to those of H5 and H6 of C4 and C6 and the other nucleobases, supporting the view that C8 tumbles independent of the duplex. In control duplex **2**, however, both H5 and H6 of C7 resonate at higher field (+0.09 and +0.08 ppm) than in **1**. Further, H5 of C1 gives a broad signal, unlike the very sharp doublet in **1**. Taken together, this indicates that C7 does have some stacking interactions with the DNA in **2** and that these are lost upon aminoacylation. An exploratory NOESY experiment with **1** at 0 °C gave broader lines for H5 of C8 and a substantial number of additional cross-peaks to W1 and A7, indicating that at very low temperature, the dangling residue is at least partially frozen out and folds onto the W1-DNA complex.

NMR-Monitored Melting Analysis. A series of one-dimensional proton NMR spectra was acquired to follow the transition from duplex to single strands. The resulting "melting curves" are plotted for selected resonances in Figure 5. It can be discerned that the shift changes for W1 are similar to those of the nucleobase protons, i.e., that a cooperative transition from a folded structure involving the tryptophan to a random coil state occurs. Further, the chemical shift changes associated with duplex dissociation are similar for the six-membered ring resonances of W1 and those of the nucleobases in the interior of the duplex and larger than those of H8 of A7, located at the 3′-terminus.

Effects of Aminoacylation on NMR Spectra of the Core Duplex. The aminoacylation has some subtle effects on the structure of the DNA duplex. At the penultimate base pair, the signal for H8 of G3 sharpens upon aminoacylation (see 1D spectra, Supporting Information). Further, in the region of the NOESY spectrum used to assign H1′ and H6/8 protons in **1** and **2** (Figure 4), an interesting difference between **1** and **2** can be discerned. For **1**, a complete set of cross-peaks is observed. In the NOESY spectrum of control DNA **2**, however, the cross-peak between H1′−T1 and H8-G2 is missing. The lack of this cross-peak between terminal nucleotides has been observed in other DNA sequences and has been ascribed to "fraying" at the terminus of the duplex (*51*). The presence of the cross-peak in **1** therefore suggests that the aminoacyl portion reduces the fraying and increases the tightness of the DNA duplex.

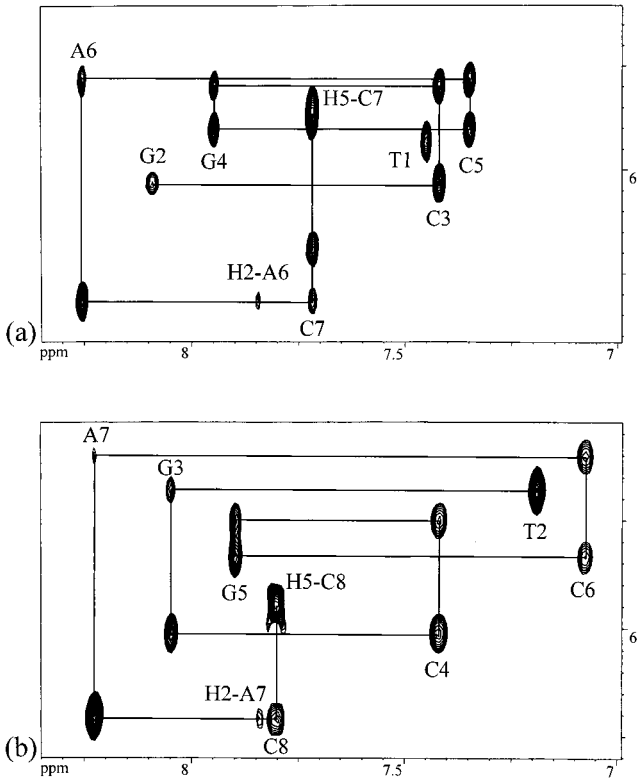

FIGURE 4: Expanded contour plots of NOESY spectra of **2** (a) and **1** (b) at 320 ms mixing time in D_2O buffer at 10 °C. NOEs establishing the connectivity are indicated by lines. Cross-peaks are between H1′ protons (5.5−6.3 ppm) and H6 (pyrimidines) or H8 (purines) protons (7.05−8.3 ppm), except for the cross-peaks labeled individually: H1′−A7 to H2-A7 and H6−C8 to H5−C8.

Structures Calculated via Restrained Molecular Dynamics. Analysis of NOESY spectra acquired at 10 °C in D_2O and H_2O/D_2O gave a total of 148 distance constraints for the symmetrical duplex, or 74 for each strand. Among these was at least one constraint for each of the protons of W1, with the exception of HZ2 and the fast-exchanging ammonium group at the amino-terminus. Not a single of the NOESY cross-peaks obtained for W1 was to a proton of G3. Together with the cross-peak from H1′−T2 to H8 of G3, this firmly rules out intercalation between penultimate and terminal base pairs.

Three-dimensional structures of **1** were calculated by restrained molecular dynamics, using the NOE-derived constraints, together with dihedral angle constraints, hydrogen bonding, and weak base pair planarity constraints (Table 4). Simulated annealing in Cartesian space (*52*) gave the same general fold, but a lower yield of low-energy structures than simulated annealing with the torsion angle molecular dynamics protocol of CNS, version 0.4 (*53*). With the latter, the structures converged to an rmsd from the average of 0.68 Å and a pairwise rmsd of coordinates of 1.2 Å for the 10 lowest energy structures, and satisfactory agreement between experimental and back-calculated NOESY spectra (Figures 6 and 7). Details of the calculational protocol and the quality of the structures are given in Tables 5 and 6. All low-energy structures are without violation of constraints, including nine intra- and nine interresidue distance constraints for W1.

The three-dimensional structure emerging from the restrained molecular dynamics shows one continuously stacked helix involving W1 as a cap on the termini. The tryptophan

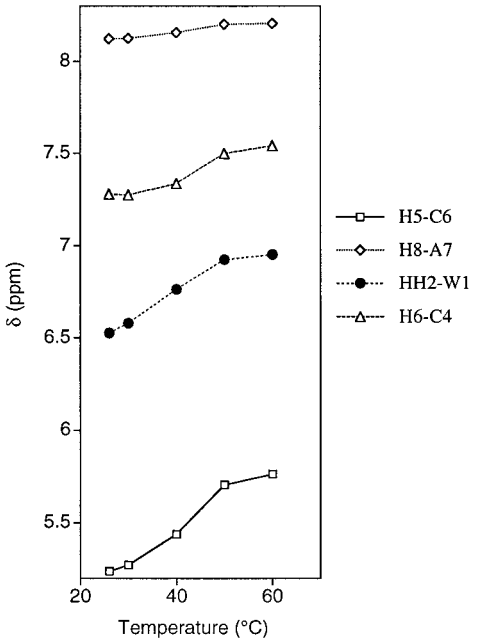

FIGURE 5: Duplex dissociation monitored by chemical shifts of selected protons from nucleobases and the indole ring of W1 in aminoacyl-DNA **1**.

residue is exclusively stacked on the T2·A7 base pair, and does not intercalate or bind in one of the grooves (Figures 8 and 9). Both the β-methylene group and the indole ring are in van der Waals contact with the nucleobases of the terminal base pair. The former touches down with one of the diastereotopic hydrogens on the thymine ring of T2, whereas the latter bridges the base pair with its six-membered ring. The conformation of the amide linker is such that the amide hydrogen of the T2-W1 linker does not engage in hydrogen bonding but packs against H6 of T2, resulting in a tightly packed arrangement of the linker without holes to be filled with solvent. Hydrogens HE1/HZ2 of W1 protrude toward the major groove, whereas HE3 and HZ3 face toward the minor groove, without reaching it or causing any NOESY cross-peaks to minor groove resonances of the penultimate base pair. The five-membered ring of A7 is not covered by the indole ring of W1, explaining why H8 of A7 is not shifted upfield relative to control duplex **2**.

Except for α and β of T2, the site of aminoacylation, and the backbone linkage to C8, the DNA adopts an unperturbed canonical B-form duplex, with dihedral angles in the expected ranges (*54*). As expected from the qualitative analysis of the NMR data (vide supra), C8, restricted by only two long-range distance constraints to H2′/2″ of A7, does not adopt an ordered state, but is disordered and preferentially localized in the vicinity of the backbone of A7.

DISCUSSION

Chemical Shifts and Line Widths of Signals. Intercalation of tryptophan, tyrosine, and phenylalanine residues of short peptides, whose nonaromatic residues anchor the aromatic residue on the DNA, has previously been proposed (*19, 20, 25*). Titrations of these intercalating peptides with polymeric DNA followed by ^{1}H NMR have invariably shown smaller upfield shifts of the aromatic tryptophan protons upon binding than those measured between low and high temperature forms of the aromatic protons of W1 in **1** (*18*−*21*),

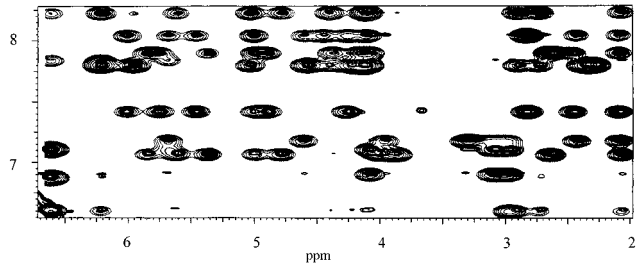

FIGURE 6: Overlay of back-calculated (gray) and experimental NOESY spectra (black) of **1**. For the back-calculation, the lowest energy structure obtained from restrained dynamics was used. The calculation was performed in X-PLOR (*52*), using the rigid body two spin approximation. Plots were generated with GIFA (*41*).

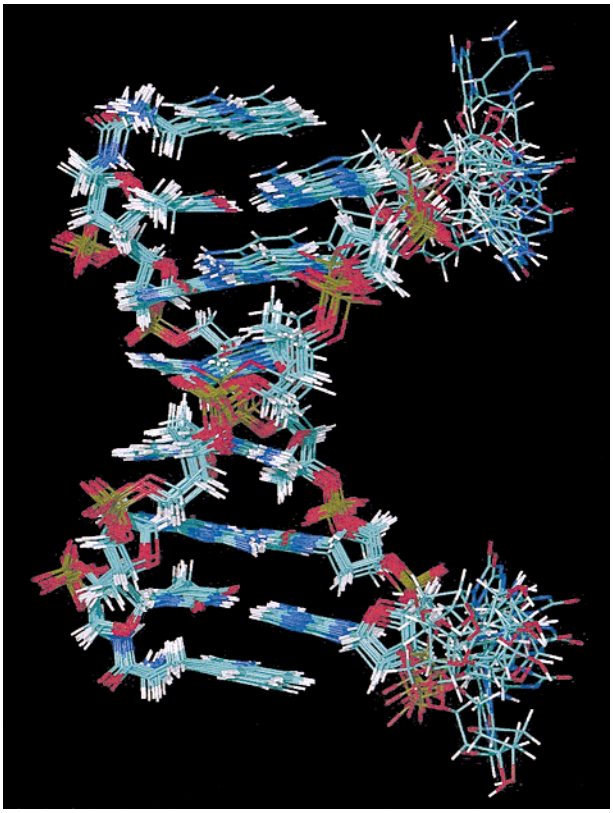

FIGURE 7: Overlay of the 10 lowest energy structures of **1** obtained from restrained torsion angle molecular dynamics. Color code: green, carbon; white, hydrogen; blue, nitrogen; red, oxygen; yellow, phosphorus. Figures 7-9 were generated with VMD (*69*).

suggesting that the stacking interactions in the peptide−DNA complexes are either not as extensive as previously thought or that the magnetic anisotropies generated by the neighboring nucleobases result in a smaller shift effect than stacking from one side only. It is noteworthy that the chemical shifts of the tryptophan residues in (KW-TGCGCAAA)$_2$ (*35*) are similar to those in **1**, indicating that the capping mode of interaction does persist in the presence of a 3′-overhang with a higher propensity to stack than a single cytidine, and does tolerate the presence of an additional amino acid residue at the amino terminus of the tryptophan.

"Capping" versus Intercalation. Several possible interaction modes were expected to be conformationally accessible to the terminal residues in **1**. Among these, an intercalation of the tryptophan between terminal and penultimate base pair (Figure 2a), together with co-intercalation or stacking of the dangling 3′-cytidine residue on the terminal base pair, would

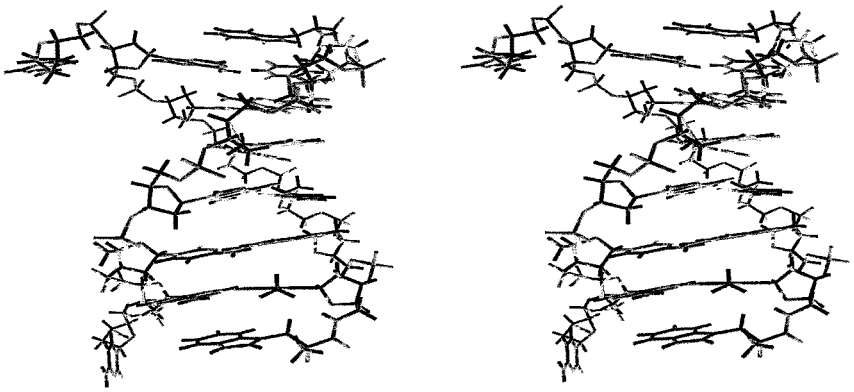

FIGURE 8: Stereoview of the lowest energy structure of **1** viewed from the minor groove.

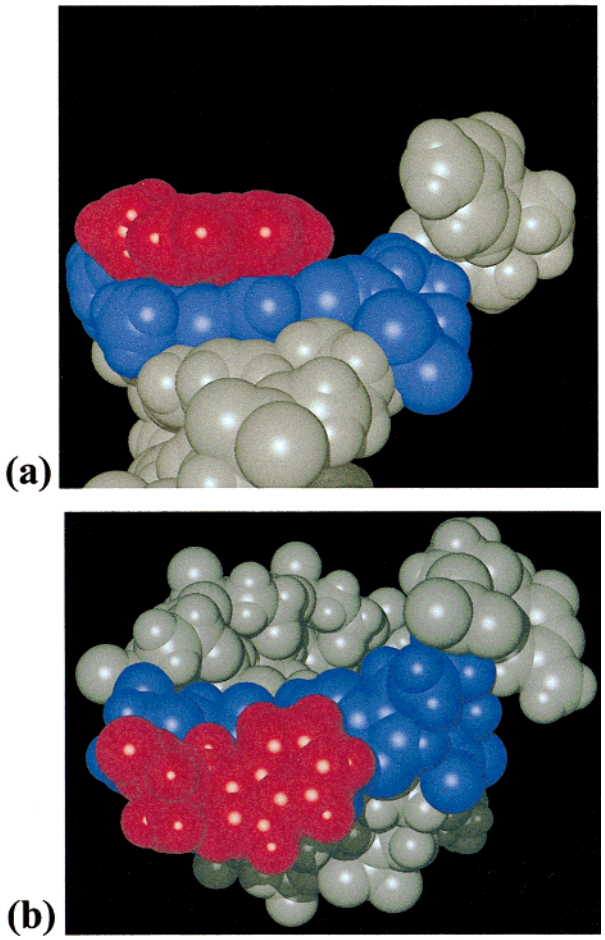

FIGURE 9: Expanded view of terminal region of the lowest energy structure of **1** in van der Waals representation. (a) View from the major groove, (b) view along the helix axis. Residue W1, red; T2 and A7, blue; remaining residues, gray.

have buried the hydrophobic surfaces of the terminal residue to the greatest extent. Free dangling aminoacyl- and C8-residues, on the other hand, would have been the least folded and most solvent-exposed structural arrangement. Neither of these two extreme conformational states appear to be populated in **1**, but stacking of the aminoacyl residue on the terminal base pair and a dangling 3′-cytidine are apparently preferred. This suggests that the attractive forces between the T2·A7 base pair and the tryptophan residue are stronger than those with the cytidine residue. The free-energy gain expected from intercalation, however, is not sufficient to disrupt the base stacking in the DNA helix and give the tryptophan indole ring access to a more hydrophobic site to be reached via intercalation. Since stacking between the terminal and penultimate base pair in our T·A-terminated duplex is already weak, as indicated by the absence of a H1′-T1 to H8-G2 NOESY cross-peak in **2**, intercalation of the indole ring of W1 should meet with a comparatively low free-energy cost. The absence of intercalation may therefore be interpreted as an indication that tryptophan is not a good intercalator.

We believe this to be true for several reasons. First, to compensate for the loss of base·base stacking, good structural complementarity between the interacting surfaces of intercalator and adjacent base pairs is required. Unlike typical intercalators, such as ethidium, proflavine, and anthracycline, which are at least tricyclic, the bicyclic indole ring is too small to cover two base pair surfaces completely. Intercalation by bicyclic aromatic rings is known (*55*, *56*), but these intercalators typically have substituents on the rings that contribute to the stacking interactions and often achieve their high affinity only via bisintercalation combined with groove binding of other portions of the molecule. The indole ring of tryptophan does not have such substituents, nor does its π-system contribute strong dipole−dipole components to the stacking interactions with nucleobases. Finally, the hydrophobicity of tryptophan residues [−0.9 on the scale of Kyte and Doolittle that ranges from 4.5 (Ile) to −4.5 (Arg)] is not great enough to provide a strong driving force for burying the indole ring in the interior of a DNA duplex.

These considerations are supported by observations of others. The intercalation of the indole ring in H-Lys-Gly-Trp-Gly-Lys-OH in double-stranded DNA has been reported to *destabilize* the duplex (*24*) and peptide binding to be more tight with a hairpin-forming sequence than with polynucleotides (*23*). The tripeptide H-Lys-Trp-Lys-OH is known to bind more tightly to single-stranded DNA, denatured DNA, and DNA containing apurinic sites than to intact double-stranded DNA (*57*, *58*), making intercalation of the indole ring as the preferred form of interaction unlikely. Tetrapeptides such as H-Arg-Trp-Arg-Arg-NH_2 and H-Lys-Trp-Lys-Lys-NH_2 also do not bind double-stranded DNA with much higher affinity than single-stranded DNA and RNA (*29*). The nucleic-acid binding cleft of single-stranded DNA-binding proteins is richer in aromatic amino acids (*10*) than that of typical double-stranded DNA-binding proteins (*59*, *60*), further supporting this point. In fact, aliphatic residues are as common in DNA intercalation wedges as aromatic residues (*7*). Together, these results suggest that it may be

misleading to think of tryptophan as a good intercalator, as also suggested by the revised solution structure of the ETS-1 complex (*2*−*5*).

Energetic and Structural Consequences of Aminoacyl "Cap". The complex whose structure was solved in this work is not stabilized by hydrogen bonds beyond those found in the control duplex **2**. Both complexes undergo cooperative transitions from double-stranded to random coil forms. Comparison of the thermodynamic data for duplex dissociation of **1** and **2** thus allows one to gauge the extent to which the tryptophanyl-cap stabilizes the duplex. Our data (Table 2) indicate that the stabilizing effect is rather slight. Even though self-complementary **1** bears two tryptophanyl residues, the effect of aminoacylation on the free energy of duplex formation is minimal, once the electrostatic stabilization by the ammonium group of W1 has been titrated out with salt. At 150 mM salt, no enthalpic stabilization of the duplex is detected, and the slight decrease in the entropic penalty for duplex formation is the only stabilizing force. This indicates that the van der Waals or π-stacking forces between the indole ring and the terminal base pair are not very strong. This seems particularly true, as the capping with the aminoacyl moiety apparently decreases the fraying of the DNA duplex at the termini and tightens the packing in the DNA portion of the duplex, adding an additional enthalpic stacking component to the total free energy of dissociation.

Again this observation is not without precedence. Mascotti and Lohman found that incorporating additional tryptophan residues into cationic peptides does not increase the affinity for single-stranded nucleic acids (*30*, *61*), i.e., that the stacking interactions and the hydrophobic effect do not suffice to cover the entropic cost for binding to single-stranded DNA. In our study on the affinity of 5′-aminoacylated, nonself-complementary oligodeoxyribonucleotides for RNA complementary strands, the ditryptophanyl sequence gave consistently lower melting points than the serinyl-tryptophanyl or lysinyl-tryptophanyl sequence (*33*).

Relevance for Stacking Interactions in Protein−*DNA and Ligand*−*DNA Complexes.* The stacking interactions between W1 and the terminal T2·A7 base pair of our complex do not appear particularly strong. One form of the noncovalent complex between 4′,6-diamidino-2-phenylindole and the DNA hexamer (CGATCG)$_2$ provides another example of a stacking interaction between an indole derivative and a terminal base pair (*62*). In this complex, the stacking interactions are probably stronger, as they suffice to assemble an *inter*molecular complex. This may be because the interaction is with a terminal C·G base pair rather than an A·T base pair or because the small molecule ligand has a larger total hydrophobic surface to offer than W1 in **1**. The strong duplex-stabilizing effect of hydrophobic nucleobase analogues appended as dangling residues suggest the latter (*63*).

5′-Aminoacylated oligoribonucleotides have recently been shown to be formed spontaneously in ribozyme-catalyzed acyl transfer reactions (*64*−*66*), making this form of aminoacylated RNA interesting in the context of evolution. Assuming that tryptophan stacks similarly on DNA and RNA duplexes, as suggested by our studies with aminoacylated oliodeoxynucleotides (*33*), 5′-aminoacylation with tryptophan will reduce the fraying of the termini in complexes with target strands. It may also have had an effect on the conformational properties of the single strand, maybe to the extent suggested for the acceptor stem of aminoacylated tRNAs (*67*). This can be expected to have consequences for molecular recognition.

Finally, one might use our results to ask larger questions about the strength of hydrophobic and π-stacking interactions in protein−DNA complexes. The attractive force resulting from stacking interactions between the tryptophan and the terminal base pair appears weak when compared to those measured for oligonucleotides acylated with gyrase inhibitors whose π-system is less electron rich (*68*). Since tryptophan is the most likely of the amino acid residues to be involved in strong π-stacking interactions, this seems to indicate that Nature did not choose to evolve a well intercalating protein residue. This is probably due to a need for specificity in binding, more difficult to achieve with intercalation than with the combination of hydrogen bonding, van der Waals interactions, and charge complementarity that is commonly found in complexes of proteins with double-stranded DNA.

CONCLUSIONS

In the aminoacylated oligonucleotide duplex (W-TGCGCAC)$_2$, the hydrophobic and stacking interactions between the side chain of tryptophan and the T·A base pair are sufficiently strong to freeze the aminoacyl residue onto the base pair and to compete with a 3′-cytidyl residue for the stacking interactions. These interactions are not strong enough, however, to produce a substantial melting point increase at physiological salt concentration, even though the aminoacyl-cap reduces the fraying of the termini of the DNA duplex. This leads to the conclusion that at least in this sequence context, the π-stacking forces between indole ring and nucleobases are weak. Besides contributing to the understanding of protein−DNA interactions, our results provide structural and thermodynamic "yardsticks" for future studies on 5′-aminoacylated nucleic acids. Our results also demonstrate that upfield shifts for the aromatic protons of tryptophan in the order of 0.5 ppm upon DNA binding do not have to be interpreted as a sign of intercalation. Instead, they may be due to stacking on exposed terminal base pairs, sticky spots in DNA that have not been widely studied.

ACKNOWLEDGMENT

The authors wish to thank S. Pochapsky, C. Turner, and J. Sudmeier for help with the acquisition of spectra, D. Daniels, C. Tetzlaff, H. Gupta, and I. Schwope for the synthesis of oligonucleotides and their purification, A. Brodsky for helpful comments on the molecular dynamics, and A. Brünger, R. Grosse-Kunstleve, and S. Stallings for making available CNS prior to its release.

SUPPORTING INFORMATION AVAILABLE

Plots of ln c_{total} versus $1/T_m$ for **1** and **2**, one-dimensional NMR spectra of **1** and **2**, a list of chemical shifts for **1** at 10 °C in phosphate-buffered saline, and coordinates of the lowest energy structure of **1**. This material is available free of charge via the Internet at http://pubs.acs.org.

REFERENCES

1. Olins, D. E., Olins, A. L., and von Hippel, P. H. (1967) *J. Mol. Biol. 24*, 157−176.

2. Werner, M. H., Clore, G. M., Fisher, C. L., Fisher, R. J., Trinh, L., Shiloach, J., and Gronenborn, A. M. (1995) *Cell 83*, 761−771.
3. Werner, M. H., Clore, G. M., Fisher, C. L., Fisher, R. J., Trinh, L., Shiloach, J., and Gronenborn, A. M. (1996) *Cell 87*, U23.
4. Werner, M. H., Gronenborn, A. M., and Clore, G. M. (1997) *Science 276*, 1957.
5. Werner, M. H., Clore, G. M., Fisher, C. L., Fisher, R. J., Trinh, L., Shiloach, J., and Gronenborn, A. M. (1997) *J. Biomol. NMR 10*, 317−328.
6. Suzuki, M. (1994) *Structure 2*, 317−326, and references therein.
7. Werner, M. H., Gronenborn, A. M., Clore, G. M. (1996) *Science 271*, 778−784.
8. Bewley, C. A., Gronenborn, A. M., and Clore, G. M. (1998) *Annu. Rev. Biophys. Biomol. Struct. 27*, 105−131, and references therein.
9. Rice, P. A., Yang, S. W., Mizuuchi, K., and Nash, H. A. (1996) *Cell 87*, 1295−1306.
10. Bochkarev, A., Pfuetzner, R. A., Edwards, A. M., and Frappier, L. (1997) *Nature 385*, 176−181, and references therein.
11. Herron, J. N., He, X. M., Ballard, D. W., Blier, P. R., Pace, P. E., Bothwell, A. L. M., Voss, E. W., and Edmundson, A. B. (1991) *Proteins: Struct., Funct., Genet. 11*, 159−175.
12. Wuttke, D. S., Foster, M. P., Case, D. A., Gottesfeld, J. M., and Wright, P. E. (1997) *J. Mol. Biol. 273*, 183−206.
13. Schevitz, R. W., Otwinowski, Z., Joachimiak, A., Lawson, C. L., and Sigler, P. B. (1985) *Nature 317*, 782−786
14. Evans, P. D., Jaseja, M., Jeeves, M., and Hyde, E. I. (1996) *Eur. J. Biochem. 242*, 567−575.
15. Russell, W. C., Newman, C., Williamson, D. H. (1975) *Nature 253*, 461−462.
16. Wilson, W. D., Tanious, F. A., Barton, H. J., Strekowski, L., Boykin, D. W., and Jones, R. L. (1989) *J. Am. Chem. Soc. 111*, 5008−5010.
17. Trotta, E., and Paci, M. (1998) *Nucleic Acids Res. 26*, 4706−4713.
18. Helene, C., and Dimicoli, J.-L. (1972) *FEBS Lett., 26*, 6−10.
19. Gabbay, E. J., Adawadkar, P. D., and Wilson, W. D., (1976) *Biochemistry 15*, 146−151.
20. Gabbay, E. J., Adawadkar, P. D., Kapicak, L., Pearce, S., and Wilson, W. D. (1976) *Biochemistry 15*, 152−157.
21. Robledo-Luiggi, C., Wilson, W. D., Pares, E., Vera, M., Martinez, C. S., Santiago, D. (1991) *Biopolymers 31*, 907−917.
22. Rajeswari, M. R. (1996) *J. Biomol. Struct. Dyn. 14*, 25−30.
23. Rajeswari, M. R., Bose, H. S., Kukreti, S., Gupta, A., Chauhan, V. S., and Roy, K. B. (1992) *Biochemistry 31*, 6237−6241.
24. Roy, K. B., Kukreti, S., Bose, H. S., Chauhan, V. S., Rajeswari, M. R. (1992) *Biochemistry 31*, 6241−6245.
25. Suzuki, M. (1990) *Nature 344*, 562−565.
26. Shine, N. R., James, T. L. (1984) *Biochemistry 24*, 4333−4341.
27. Sartorius, J., Schneider, H. J. (1995) *FEBS Lett. 374*, 387−392.
28. Mihara, Y., Doi, M., Inohara, T., Kawamura, M., Hamanaka, N., and Ishida, T. (1997) *Biochem. Biophys. Res. Commun. 24*, 803−806.
29. Mascotti, D. P., and Lohman, T. M. (1997) *Biochemistry 36*, 7272−7279.
30. Mascotti, D. P., and Lohman, T. M. (1993) *Biochemistry 32*, 10568−10579.
31. Padmanabhan, S., Zhang, W. T., Capp, M. W., Anderson, C. F., and Record, M. T. (1997) *Biochemistry 36*, 5193−5206.
32. Zhang, W., Bond, J. P., Anderson, C. F., Lohman, T. M., and Record, M. T. (1996) *Proc. Natl. Acad. Sci. U.S.A. 93*, 2511−2516.
33. Sarracino, D. A., Steinberg, J. A., Vergo, M. T., Woodworth, G. F., Tetzlaff, C. N., and Richert, C. (1998) *Bioorg. Med. Chem. Lett. 8*, 2511−2516.
34. Brown, P. E. (1970) *Biochim. Biophys. Acta 213*, 282−289.
35. Tetzlaff, C. N., Schwope, I., Bleczinski, C. F., Steinberg, J. A., and Richert, C. (1998) *Tetrahedron Lett. 39*, 4215−4218.
36. Marky, L. A., and Breslauer, K. J. (1987) *Biopolymers 26*, 1601−1620.
37. Sklenar, V., Piotto, M., Leppik, R., and Saudek, V. (1993) *J. Magn. Res. Ser. A 102*, 241−245.
38. Kumar, A., Ernst, R. R., and Wüthrich, K. (1980) *Biochem. Biophys. Res. Commun. 95*, 1−6.
39. Bax, A., and Davis, D. G. (1985) *J. Magn. Reson. 65*, 355−360.
40. Piantini, U., Sørensen, O. W., and Ernst, R. R. (1982) *J. Am. Chem. Soc. 104*, 6800−6801.
41. Delsuc, M. A. (1989) in *Maximum Entropy and Bayesian Methods* (Skilling, J., Ed.) pp 285−290, Kluwer Academic: Dordrecht, The Netherlands.
42. Marion, D., and Wüthrich, K. (1983) *Biochem. Biophys. Res. Commun. 113*, 967−974.
43. Wijmenga, S. S., Mooren, M. M. W., and Hilbers, C. W. (1993) in *NMR of Macromolecules, A Practical Approach* (Roberts, G. C. K., Ed.) pp 217−288, Oxford University Press, Oxford, U.K.
44. Calculated with a program written in house, using parameters reported in SantaLucia, J., Allawi, H. T., and Seneviratne, A. (1996) *Biochemstry 35*, 3555−3562.
45. Vesnaver, G., and Breslauer, K. J. (1991) *Proc. Natl. Acad. Sci. U.S.A. 88*, 3569−3573.
46. Scheek, R. M., Boelens, R., Russo, N., van Boom, J. H., and Kaptein, R. (1984) *Biochemistry 23*, 1371−1376.
47. Feigon, J., Leupin, W., Denny, W. A., and Kearns, D. R. (1983) *Biochemistry 22*, 5943−5951.
48. Patel, D. J., Shapiro, L., and Hare, D. (1986) *J. Biol. Chem. 261*, 1223−1229.
49. Walters, K. J., and Russu, I. M. (1993) *Biopolymers 22*, 943−951.
50. Davies, D. B. (1978) *Prog. NMR-Spectrosc. 12*, 135−225.
51. Hare, D. R., Wemmer, D. E., Chou, S.-H., and Drobny, G. (1983) *J. Mol. Biol. 171*, 319−336.
52. A. T. Brünger (1992) X-PLOR, version 3.1, *X-PLOR Manual*, Yale University Press, New Haven, CT.
53. Stein, E. G., Rice, L. M., and Brünger, A. T. (1997) *J. Magn. Reson., Ser. B 124*, 154−164.
54. Saenger, W. (1984) *Principles of Nucleic Acid Structure*, Springer, New York.
55. Boger, D. L., Chen, J. H., and Saionz, K. W. (1996) *J. Am. Chem. Soc. 118*, 1629−1644.
56. Chen, H. F., and Patel, D. J. (1995) *J. Mol. Biol. 246*, 164−179.
57. Toulme, J.-J., and Helene, C. (1977) *J. Biol. Chem. 252*, 244−249.
58. Behmoaras, T., Toulme, J. J., and Helene, C. (1981) *Nature 292*, 858−859.
59. Choo, Y., and Klug, A. (1997) *Curr. Opin. Struct. Biol. 7*, 117−125.
60. Mandel-Gutfreund, Y., and Margalit, H. (1998) *Nucleic Acids Res. 26*, 2306−2312.
61. Mascotti, D. P., and Lohman, T. M. (1992) *Biochemistry 31*, 8932−8946.
62. Trotta, E., D'Ambrosio, E., Ravagnan, G., and Paci. M. (1996) *J. Biol. Chem. 271*, 27608−27614.
63. Guckian, K. M., Schweitzer, B. A., Ren, R. X.-F., Sheils, C. J., Paris, P. L., Tahmassebi, D. C., and Kool, E. T. (1996) *J. Am. Chem. Soc. 118*, 8182−8283.
64. Lohse, P. A., and Szostak, J. W. (1996) *Nature 381*, 442−444
65. Hager, A. J., Pollard, J. D., and Szostak, J. W. (1996) *Chem. Biol. 3*, 717−725.
66. Suga, H., Lohse, P. A., and Szostak, J. W. (1998) *J. Am. Chem. Soc. 120*, 1151−1156.
67. Limmer, S., Hofmann, H. P., Ott, G., and Sprinzl, M. (1993) *Proc. Natl. Acad. Sci. U.S.A. 90*, 6199−6202.
68. Schwope, I., Altman, R. K., Stitelman, D. H., and Richert, C. Unpublished results.
69. Humphrey, W., Dalke, A., and Schulten, K. (1996) *J. Mol. Graphics 14*, 33−38.

BI991169W